***The following resources related to this article are available online at
www.sciencemag.org (this infomation is current as of September 1, 2011):***

Updated information and services, including high-resolution figures, can be found in the online version of this article at:
http://www.sciencemag.org/content/333/6047/1279.full.html

Supporting Online Material can be found at:
http://www.sciencemag.org/content/suppl/2011/08/31/333.6047.1279.DC1.html

This article **cites 33 articles**, 9 of which can be accessed free:
http://www.sciencemag.org/content/333/6047/1279.full.html#ref-list-1

This article appears in the following **subject collections:**
Chemistry
http://www.sciencemag.org/cgi/collection/chemistry

6. J. Vermant, M. J. Solomon, *J. Phys. Condens. Matter* **17**, R187 (2005).
7. J. M. Brader, *J. Phys. Condens. Matter* **22**, 363101 (2010).
8. D. R. Foss, J. F. Brady, *J. Fluid Mech.* **407**, 167 (2000).
9. J. R. Melrose, R. C. Ball, *J. Rheol. (N.Y.N.Y.)* **48**, 961 (2004).
10. H. M. Laun *et al.*, *J. Rheol. (N.Y.N.Y.)* **36**, 743 (1992).
11. B. J. Maranzano, N. J. Wagner, *J. Chem. Phys.* **117**, 10291 (2002).
12. D. Kalman, N. J. Wagner, *Rheol. Acta* **48**, 897 (2009).
13. R. L. Hoffman, *J. Colloid Interface Sci.* **46**, 491 (1974).
14. R. L. Hoffman, *J. Rheol. (N.Y.N.Y.)* **42**, 111 (1998).
15. C. B. Holmes, M. E. Cates, M. Fuchs, P. Sollich, *J. Rheol. (N.Y.N.Y.)* **49**, 237 (2005).
16. D. Lootens, H. van Damme, Y. Hémar, P. Hébraud, *Phys. Rev. Lett.* **95**, 268302 (2005).
17. A. Fall, N. Huang, F. Bertrand, G. Ovarlez, D. Bonn, *Phys. Rev. Lett.* **100**, 018301 (2008).
18. E. Brown *et al.*, *Nat. Mater.* **9**, 220 (2010).
19. E. Brown, H. M. Jaeger, Preprint at http://arxiv.org/abs/1010.4921 (2010).
20. Y. L. Wu, D. Derks, A. van Blaaderen, A. Imhof, *Proc. Natl. Acad. Sci. U.S.A.* **106**, 10564 (2009).
21. L. Isa, R. Besseling, A. B. Schofield, W. C. K. Poon, *Adv. Polym. Sci.* **236**, 163 (2010).
22. K. M. Schmoller, P. Fernández, R. C. Arevalo, D. L. Blair, A. R. Bausch, *Nat. Commun.* **1**, 134 (2010).
23. Materials and methods are available as supporting material on *Science* Online.
24. C. R. Nugent, K. V. Edmond, H. N. Patel, E. R. Weeks, *Phys. Rev. Lett.* **99**, 025702 (2007).
25. F. Parsi, F. Gadala-Maria, *J. Rheol. (N.Y.N.Y.)* **31**, 725 (1987).
26. C. Gao, S. D. Kulkarni, J. F. Morris, J. F. Gilchrist, *Phys. Rev. E Stat. Nonlin. Soft Matter Phys.* **81**, 041403 (2010).
27. J. F. Brady, G. Bossis, *J. Fluid Mech.* **155**, 105 (1985).
28. M. Urbakh, J. Klafter, D. Gourdon, J. Israelachvili, *Nature* **430**, 525 (2004).

Traffic Jams Reduce Hydrolytic Efficiency of Cellulase on Cellulose Surface

Kiyohiko Igarashi,[1]*† Takayuki Uchihashi,[2,3,4]* Anu Koivula,[5] Masahisa Wada,[1,6] Satoshi Kimura,[1,6] Tetsuaki Okamoto,[1,2] Merja Penttilä,[5] Toshio Ando,[2,3,4] Masahiro Samejima[1]

A deeper mechanistic understanding of the saccharification of cellulosic biomass could enhance the efficiency of biofuels development. We report here the real-time visualization of crystalline cellulose degradation by individual cellulase enzymes through use of an advanced version of high-speed atomic force microscopy. *Trichoderma reesei* cellobiohydrolase I (*Tr*Cel7A) molecules were observed to slide unidirectionally along the crystalline cellulose surface but at one point exhibited collective halting analogous to a traffic jam. Changing the crystalline polymorphic form of cellulose by means of an ammonia treatment increased the apparent number of accessible lanes on the crystalline surface and consequently the number of moving cellulase molecules. Treatment of this bulky crystalline cellulose simultaneously or separately with *T. reesei* cellobiohydrolase II (*Tr*Cel6A) resulted in a remarkable increase in the proportion of mobile enzyme molecules on the surface. Cellulose was completely degraded by the synergistic action between the two enzymes.

B iorefining encompasses production of fuels, power, heat, and value-added chemicals by appropriate conversion of ligno-cellulosic feedstocks. This prospect offers many advantages, including diminished carbon dioxide emission, productive use of renewable nonfood crops or inedible waste products, and reduction of petroleum use. One of the bottlenecks to widespread biorefining application is the enzymatic hydrolysis of the cellulosic raw material into sugars. In attempts to maximize efficiency and reduce costs, many studies on both individual cellulases and enzyme cocktails have been carried out (*1*). Various pretreatment methods have also been examined to increase the amount of sugar generated from cellulosic biomass with reduced enzyme loading and energy consumption, aiming at the development of commercially viable bioprocesses. It is generally recognized that one of the problems in cellulose hydrolysis is the slowdown of enzyme action with time and conversion (*2*, *3*). Cellulose is a major component of plant cell walls, accounting for almost half of their net weight. Cell wall cellulose typically has ~70% crystallinity, suggesting that approximately one-third of net cellulosic biomass consists of natural crystalline cellulose, which is generally called cellulose I (*4*). Because cellulose chains have stable β-1,4-glucosidic bonds and each chain is also stabilized by intra- and intermolecular hydrogen bonds, cellulose I is quite resistant not only to chemical hydrolysis but also to enzymatic degradation (*5*).

The industrially important cellulolytic ascomycete fungus *Trichoderma reesei* (anamorph of *Hypocrea jecorina*) secretes two extracellular cellobiohydrolases (CBHs), which are cellulases that can hydrolyze glycosidic linkages particularly at a crystalline surface, and form cellobiose (β-1,4-glucosidic dimer) as a major product from cellulose I (*6*). The two *T. reesei* CBHs hydrolyze crystalline cellulose from the reducing and non-reducing ends, respectively (*7*). These enzymes have a similar two-domain organization: The cellulose-binding domain (CBD), which is categorized into carbohydrate-binding module (CBM) family 1, contributes to adsorption on the insoluble substrate, and the cellulose-hydrolyzing catalytic domain (CD) catalyzes cleavage of glycosidic bonds. The two *T. reesei* cellobiohydrolase CDs have different types of folds. The CD of CBH I belongs to the glycoside hydrolase (GH) family 7, and the CD of CBH II belongs to the GH family 6, as listed on the Carbohydrate-Active enZyme (CAZy) server (*8*), and thus, the two enzymes are called *Tr*Cel7A and *Tr*Cel6A, respectively. In both cellobiohydrolases, the catalytic amino acids are located in a relatively long tunnel formed by surface loops extending from the central fold of the CD (*9*, *10*). We previously visualized the linear movement of wild-type and isolated CD on cellulose I$_\alpha$ using high-speed atomic force microscopy (HS-AFM); the data suggested that the sliding movement of wild-type *Tr*Cel7A reflects the processive degradation of the cellulose chain by catalysis at the CD and requires initial recognition of the cellulose chain. The chain recognition involves the tryptophan residue W40 at the entrance of the *Tr*Cel7A active site tunnel (*11*).

In the present study, we succeeded in enhancing the temporal and spatial resolutions by using a laboratory-built HS-AFM with extensive improvements over the version reported previously (*12*), and we were able to visualize the movement of *Tr*Cel7A molecules on crystalline cellulose in detail. Enzyme molecules sliding

[1]Department of Biomaterial Sciences, Graduate School of Agricultural and Life Sciences, University of Tokyo, Bunkyo-ku, Tokyo 113-8657, Japan. [2]Department of Physics, Kanazawa University, Kanazawa 920-1192, Japan. [3]Bio-AFM Frontier Research Center, College of Science and Engineering, Kanazawa University, Kakuma-machi, Kanazawa 920-1192, Japan. [4]Core Research for Evolutional Science and Technology, Japan Science and Technology Agency, Sanbon-cho, Chiyoda-ku, Tokyo 102-0075, Japan [5]VTT Technical Research Centre of Finland, Post Office Box 1000, FI-02044 VTT, Finland. [6]Department of Plant and Environmental New Resources, College of Life Sciences, Kyung Hee University, 1, Seocheon-dong, Giheung-ku, Yongin-si, Gyeonggi-do 446-701, Republic of Korea.

*These authors contributed equally to this work.
†To whom correspondence should be addressed. E-mail: aquarius@mail.ecc.u-tokyo.ac.jp (K.I.)

unidirectionally on the cellulose I_α surface are shown in Fig. 1A and movie S1. This movement of TrCel7A was observed only at the top of the cellulose crystal, where the individual enzyme molecules were moving as one line. The movement of the TrCel7A molecules was analyzed by using a custom software to track the linear movement of the center of each molecule, and the time course of molecular movement is shown in Fig. 1B. Some molecules slid continuously without stopping (demonstrated by the orange plot in Fig. 1B), whereas the movement of other TrCel7A molecules was often disturbed by halted and/or more slowly moving molecules (demonstrated by the open green and closed red plots in Fig. 1B), resembling the movement of traffic on a road. According to the histogram of the measured velocities (Fig. 1C), there would seem to be two populations of TrCel7A molecules having average velocities of -0.32 ± 3.4 and 7.1 ± 3.9 nm/s. This is consistent with the idea that TrCel7A molecules intermittently repeat stop and go movements.

It is generally believed that CBHs have two modes of adsorption on a cellulose surface: the productive adsorption mode, in which both the CD and CBD contribute to the binding, and the nonproductive adsorption mode, in which the enzyme molecules bind only via the CBD (13). In our previous HS-AFM study with TrCel7A and its mutants, that variant that bound only via the CBD (W40A without tryptophan residue at the active-site entrance) did not remain long on the surface and therefore could not be continuously visualized (11). In contrast, molecules bound to the substrate chain via the CD (the TrCel7A wild-type enzyme, isolated CD without CBD, and the inactive mutant E212Q) could be continuously visualized during HS-AFM observation. Considering these results, it seems likely that the TrCel7A molecules visualized here as stationary in the middle of cellulose fibrils have been stopped while holding a substrate chain in the active site tunnel of the CD. Moreover, we previously reported an average velocity of 3.5 ± 1.1 nm/s for the movement of TrCel7A (11), as shown by a dotted line in Fig. 1B. The velocity of moving molecules obtained in the present study was 7.1 ± 3.9 nm/s—twice the velocity estimated in the previous study—whereas the averaged velocity for all molecules (stopped and moving) was 5.3 ± 4.9 nm/s. Therefore, it seems likely that this earlier value (for average velocity) was determined by the two populations of moving and stopped molecules. Although the time-resolution of the HS-AFM observation used in this study was up to 300 ms/frame, greater than three times faster than that in the previous work (up to 1 s/frame), this time-resolution is still not high enough to analyze each hydrolytic step of TrCel7A. If one hydrolytic cycle produces one cellobiose unit, which is approximately 1 nm in length, each individual hydrolysis-related movement could occur within 140 ms, as calculated from the velocity obtained in the present study.

As already mentioned, cellulose I is quite resistant to enzymatic hydrolysis. We have shown recently that crystalline polymorphic conversion from cellulose I to cellulose III_I through supercritical ammonia treatment dramatically enhances the hydrolysis of crystalline cellulose by TrCel7A (14). In order to investigate the reason for the enhanced hydrolysis of cellulose III_I, the degradation of the crystalline celluloses was visualized with HS-AFM, and the results were compared with those of the conventional adsorption study. The binding isotherms—plots of free enzyme concentration versus amount of adsorbed enzyme ([F]-A)—followed a Langmuir-type two-binding site model on both crystalline celluloses (cellulose I_α and III_I) (Fig. 2A). These data show that TrCel7A has higher binding capacity to cellulose III_I than to cellulose I_α. The simulated curves were divided into high-affinity (solid line) and low-affinity (dashed line) components, as shown in Fig. 2B. There was
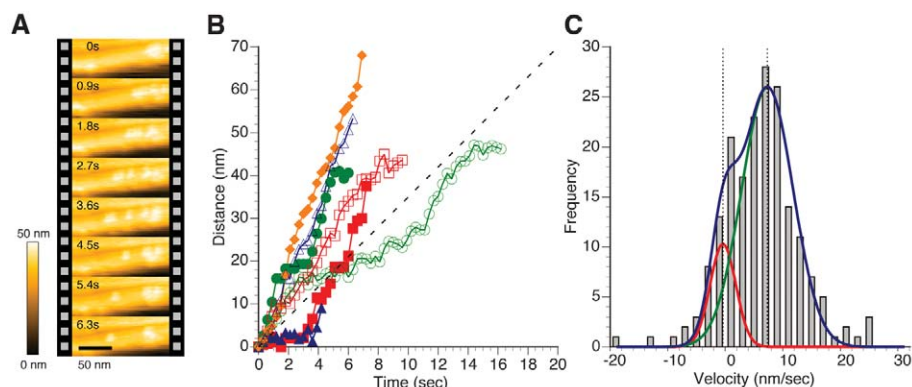

Fig. 1. (**A**) Real-time observation of crystalline cellulose I_α incubated with TrCel7A by means of HS-AFM. The time interval between images is 0.9 s. These images are taken from movie S1. (**B**) Time course of distance from the initial position for TrCel7A molecules. The mobility of each molecule was analyzed by using a routine developed in Igor Pro software, as described in the supporting online material. The different symbols indicate different molecules observed in HS-AFM images. The black dotted line represents the average velocity of TrCel7A (3.5 nm/s) estimated from previous HS-AFM observation (11). (**C**) Velocity distribution of the linear movement of TrCel7A on crystalline cellulose I_α ($n = 188$ xxxxx). The histogram was approximated by the combination of two Gaussian distribution curves (blue line) with mean $\pm$ SD values of -0.32 ± 3.4 (red) and 7.1 ± 3.9 (green).
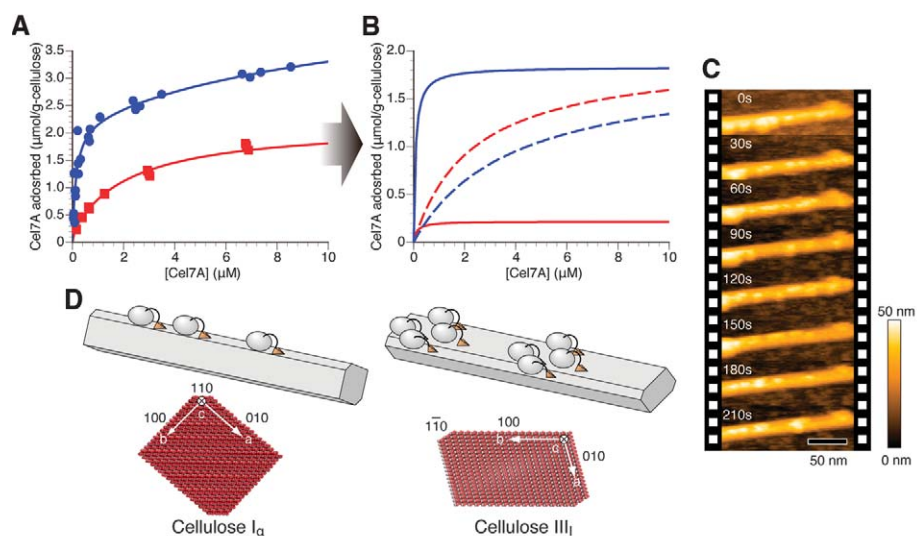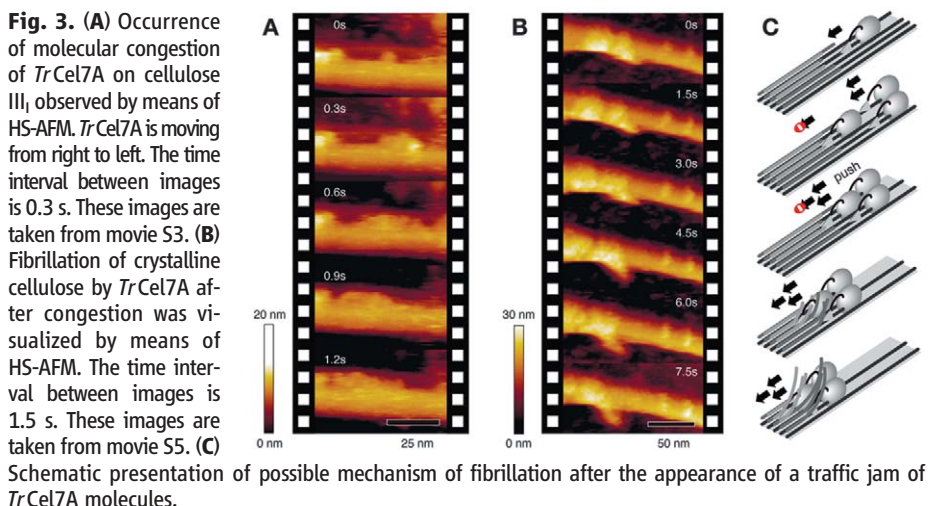

Fig. 2. (**A**) Free TrCel7A concentration dependence of the amount of adsorbed enzyme on crystalline cellulose I_α (red) and III_I (blue). These plots were fitted to curves (red and blue solid lines) simulated by use of Langmuir's two-binding-site model, as described in (26); the high- (solid line) and low-affinity (dashed line) binding curves are individually drawn in (**B**). The binding parameters (A_1, K_{ad1}, A_2, and K_{ad2}) of TrCel7A for cellulose I_α were 0.22 ± 0.02, 8.4 ± 1.4, 2.0 ± 0.2, and 0.44 ± 0.09, and those for cellulose III_I were 1.9 ± 0.1, 11 ± 2, 1.8 ± 0.3, and 0.31 ± 0.06 (mean $\pm$ SD), respectively. (**C**) HS-AFM images of crystalline cellulose III_I degradation by TrCel7A. The time interval between images is 30 s. These images are taken from movie S2. (**D**) Schematic presentation of the increased number of observed lanes for TrCel7A on cellulose I_α (top left) compared with cellulose III_I (top right) and comparison of sections of crystalline cellulose I_α (bottom left) and cellulose III_I (bottom right) according to previous reports (17, 18).
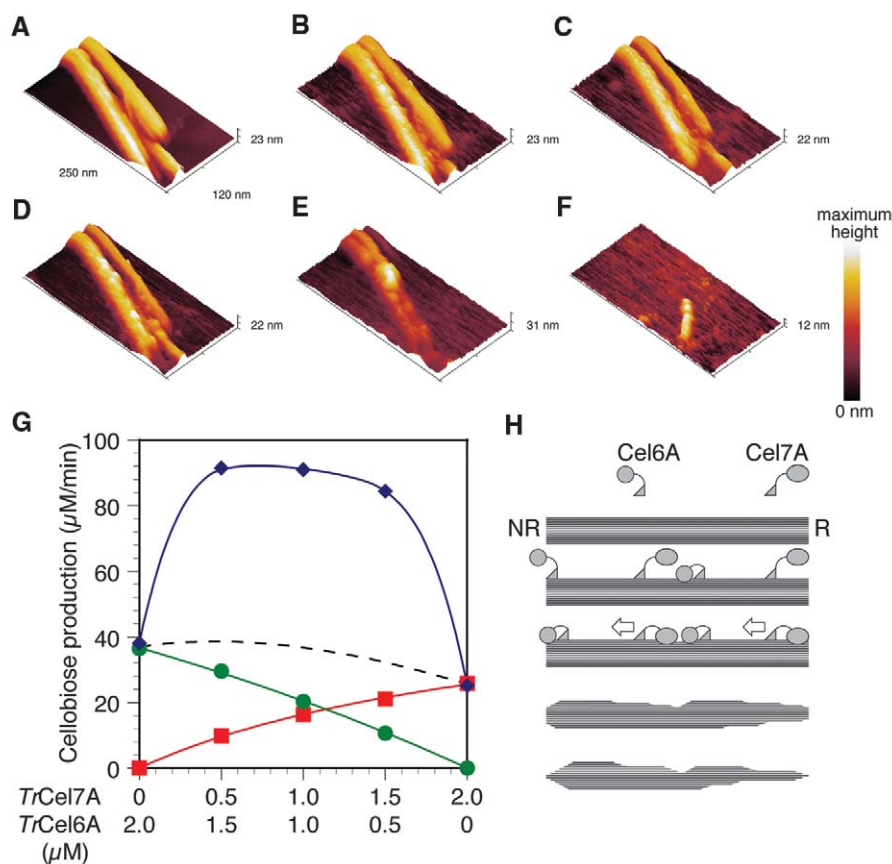
no apparent difference in the low-affinity component between the two crystalline polymorphs, whereas the high-affinity component in the case of crystalline cellulose III_I was quite large compared with that of crystalline cellulose I_α, which is consistent with our previous study (*14*).

Fig. 3. (**A**) Occurrence of molecular congestion of TrCel7A on cellulose III_I observed by means of HS-AFM. TrCel7A is moving from right to left. The time interval between images is 0.3 s. These images are taken from movie S3. (**B**) Fibrillation of crystalline cellulose by TrCel7A after congestion was visualized by means of HS-AFM. The time interval between images is 1.5 s. These images are taken from movie S5. (**C**) Schematic presentation of possible mechanism of fibrillation after the appearance of a traffic jam of TrCel7A molecules.

Fig. 4. Synergistic hydrolysis by TrCel6A and TrCel7A visualized by means of HS-AFM. (**A**) Microfibrils of cellulose III_I observed on the highly oriented pyrolytic graphite surface. (**B** and **C**) Images after 3.0 min (B) and 8.0 min (C) from the addition of 2.0 µM TrCel7A. (**D** to **F**) Images after 0.5 min (D), 2.5 min (E), and 4.5 min (F) from the addition of TrCel7A after incubation with TrCel6A for 495 s. (A) to (C) and (D) to (F) are acquired from movies S8 and S9, respectively. The numbers attached to the z axes, which correspond to the maximum height in the lookup table (LUT), represent the maximum heights of the respective images. (**G**) Synergy between TrCel6A and TrCel7A in cellobiose production from cellulose III_I. Green and red plots are the rates of cellobiose production by TrCel6A and TrCel7A, respectively, and the blue plot shows the synergy between the two enzymes. The dotted line indicates the simple sum of cellobiose production calculated from the green and red plots. (**H**) Proposed mechanism for the exo-exo synergy between TrCel6A and TrCel7A.

When the hydrolysis of crystalline cellulose III_I by TrCel7A was observed with HS-AFM, as shown in Fig. 2C and movie S2, differences were apparent in the number but not in the velocity of enzyme molecules moving on cellulose III_I and cellulose I_α. In the case of crystalline cellulose I_α, enzyme molecules slid only along limited lanes (Fig. 1A and movie S1), whereas on cellulose III_I, TrCel7A molecules moved over almost the whole surface. This may reflect the difference in the amount of high-affinity binding (Fig. 2, A and B). Lehtiö and co-workers reported recently that the isolated CBD of TrCel7A binds to the 110 surface of *Valonia* cellulose (cellulose I_α), and they suggested that TrCel7A degrades crystalline cellulose from this hydrophobic surface (*15*). The hypothesis was recently confirmed by means of AFM observation (*16*). The characteristics of cellulose I_α and III_I differ (*17*, *18*) in that cellulose I_α bears hydrophobic 110 surfaces between hydrophilic 100 and 010 surfaces, whereas cellulose III_I has similarly hydrophobic $1\bar{1}0$ and hydrophilic 010 surfaces but moderately hydrophobic (and larger) 100 surfaces, as shown in Fig. 2D. Because we used hydrophobic highly oriented pyrolytic graphite as a grid in the experiments, the crystals are expected to be oriented with their hydrophobic surfaces in contact with it and by symmetry on the opposite, top face as well. Therefore, it appears that TrCel7A moved not only on the hydrophobic $1\bar{1}0$ surface but also on the (somewhat less) hydrophobic 100 surface of cellulose III_I. In contrast, 110 is the only surface sufficiently hydrophobic for the enzyme to attach to in the case of cellulose I_α. Increasing the number of suitable lanes for cellulase movement would be an effective way to enhance crystalline cellulose hydrolysis, as judged from the comparison between cellulose I_α and cellulose III_I. In the case of TrCel7A action, moreover, when the movement of one molecule was halted many following molecules stacked behind it on the cellulose III_I surface, causing a traffic jam, as shown in Fig. 3A and movie S3. In Fig. 3B and movies S4 and S5, however, it becomes clear that after several additional molecules had also become blocked the enzyme molecules started to move again on the surface, and a cellulose bundle was peeled off from the crystalline cellulose. This behavior may reflect the presence of an obstruction on the surface of crystalline cellulose, which a single TrCel7A molecule is unable to climb over and is therefore halted. However, as schematically represented in Fig. 3C the accumulation of subsequent molecules behind the blocked molecule seems to lead to elimination of the obstacle (or obstacles). As a result, the blocked molecules restart linear movement from the point where the first molecule had stopped.

In the process of crystalline cellulose hydrolysis by *T. reesei*, two major cellobiohydrolases, TrCel7A and TrCel6A, synergistically contribute as described above (*7*, *19*). We imaged the hydrolytic processes with crystalline cellulose III_I

in the presence of both TrCel6A and TrCel7A. The crystals were first observed without enzyme (Fig. 4A and movie S6) then incubated TrCel6A for 495 s (Fig. 4, B and C, and movies S7 and S8), and the same crystalline cellulose was again visualized after further addition of TrCel7A (Fig. 4, D to F, and movies S7 and S9). As shown in Fig. 4, A to C, and movie S8, the appearance of the cellulose crystals did not change during incubation with TrCel6A, although many enzyme molecules were observed on the surfaces. When TrCel7A was added, enzyme molecules were seen to start moving from many points on the surface of the substrate, and the crystals apparently became thinner after the passage of the enzyme molecules, as shown in Fig. 4, D to F, and movie S9. This degradation of crystalline cellulose was dramatically faster than was the case with TrCel7A alone (movie S2).

We also examined this synergetic action between the two enzymes biochemically. Cellobiose production from the reaction mixture containing both TrCel6A and TrCel7A (Fig. 4G, blue line) was greater than the sum (dotted line) of production by the individual enzymes separately (green and red lines for TrCel6A and TrCel7A, respectively), confirming the occurrence of synergistic hydrolysis of crystalline cellulose by these two enzymes, which is in agreement with previous findings. This has been called exo-exo synergy (20). These two enzymes both have active sites located in a tunnel that passes through the whole CD. The active site tunnel of TrCel6A is formed by two surface loops and is about 20 Å long, whereas that of TrCel7A is approximately 50 Å long, comprising six loops (9, 10, 21, 22). Previous transmission electron microscopic observations of crystalline cellulose after hydrolysis by TrCel6A and TrCel7A demonstrated that the two enzymes degrade the substrate from different ends of the crystal; TrCel7A degrades the substrate from the reducing end, leading to fibrillation, thinning of the crystal, or narrowing of the crystal end,

whereas TrCel6A hydrolyzes the cellulose chain from the nonreducing end less processively than TrCel7A, sharpening the crystal tip (23, 24). It is somewhat difficult to find an explanation for this type of synergistic action on highly crystalline cellulose. One possibility is that the two loops forming the active site tunnel of TrCel6A can open and allow generation of nicks in the middle of crystalline cellulose and that these nicks become starting and ending points for TrCel7A activity. This mode of synergistic action (schematically shown in Fig. 4H) could also be called endo-exo synergy (25), although as explained above, TrCel6A is generally defined as an exo-glucanase (cellobiohydrolase). The synergistic hydrolysis was also observed when TrCel7A and TrCel6A were incubated at the same time with cellulose III$_I$.

The present results suggest that the roughness of the crystalline cellulose surface leads to the formation of traffic jams of productively bound cellulases. Thus, flattening the surface, removing obstacles, and/or increasing the number of lanes, entrances, and exits by means of pretreatment or combined use of synergistically acting enzymes should reduce the molecular congestion, improving the mobility of the cellulase molecules and increasing the efficiency of hydrolysis.

References and Notes
1. M. E. Himmel et al., Science 315, 804 (2007).
2. J. Jalak, P. Väljamäe, Biotechnol. Bioeng. 106, 871 (2010).
3. B. Yang, D. M. Willies, C. E. Wyman, Biotechnol. Bioeng. 94, 1122 (2006).
4. D. N. S. Hon, Cellulose 1, 1 (1994).
5. R. Wolfenden, Y. Yuan, J. Am. Chem. Soc. 130, 7548 (2008).
6. T. T. Teeri, Trends Biotechnol. 15, 160 (1997).
7. T. T. Teeri et al., Biochem. Soc. Trans. 26, 173 (1998).
8. B. Henrissat, A. Bairoch, Biochem. J. 293, 781 (1993).
9. C. Divne et al., Science 265, 524 (1994).
10. J. Rouvinen, T. Bergfors, T. Teeri, J. K. Knowles, T. A. Jones, Science 249, 380 (1990).
11. K. Igarashi et al., J. Biol. Chem. 284, 36186 (2009).
12. T. Ando et al., Proc. Natl. Acad. Sci. U.S.A. 98, 12468 (2001).
13. J. Ståhlberg, G. Johansson, G. Pettersson, Biotechnology (N. Y.) 9, 286 (1991).
14. K. Igarashi, M. Wada, M. Samejima, FEBS J. 274, 1785 (2007).
15. J. Lehtiö et al., Proc. Natl. Acad. Sci. U.S.A. 100, 484 (2003).
16. Y. S. Liu et al., J. Biol. Chem. 286, 11195 (2011).
17. M. Wada, H. Chanzy, Y. Nishiyama, P. Langan, Macromolecules 37, 8548 (2004).
18. Y. Nishiyama, J. Sugiyama, H. Chanzy, P. Langan, J. Am. Chem. Soc. 125, 14300 (2003).
19. L. E. R. Berghem, L. G. Pettersson, U. B. Axiofredriksson, Eur. J. Biochem. 53, 55 (1975).
20. B. Nidetzky, W. Steiner, M. Hayn, M. Claeyssens, Biochem. J. 298, 705 (1994).
21. C. Divne, J. Ståhlberg, T. T. Teeri, T. A. Jones, J. Mol. Biol. 275, 309 (1998).
22. A. Koivula et al., J. Am. Chem. Soc. 124, 10015 (2002).
23. H. Chanzy, B. Henrissat, FEBS Lett. 184, 285 (1985).
24. T. Imai, C. Boisset, M. Samejima, K. Igarashi, J. Sugiyama, FEBS Lett. 432, 113 (1998).
25. T. M. Wood, S. I. McCrae, Biochem. J. 171, 61 (1972).
26. K. Igarashi, M. Wada, R. Hori, M. Samejima, FEBS J. 273, 2869 (2006).

Supporting Online Material
www.sciencemag.org/cgi/content/full/333/6047/1279/DC1
Materials and Methods
References (27–33)
Movies S1 to S9

Isotopic Signature of N$_2$O Produced by Marine Ammonia-Oxidizing Archaea

Alyson E. Santoro,[1]*† Carolyn Buchwald,[2] Matthew R. McIlvin,[1] Karen L. Casciotti[1]*‡

The ocean is an important global source of nitrous oxide (N$_2$O), a greenhouse gas that contributes to stratospheric ozone destruction. Bacterial nitrification and denitrification are thought to be the primary sources of marine N$_2$O, but the isotopic signatures of N$_2$O produced by these processes are not consistent with the marine contribution to the global N$_2$O budget. Based on enrichment cultures, we report that archaeal ammonia oxidation also produces N$_2$O. Natural-abundance stable isotope measurements indicate that the produced N$_2$O had bulk δ^{15}N and δ^{18}O values higher than observed for ammonia-oxidizing bacteria but similar to the δ^{15}N and δ^{18}O values attributed to the oceanic N$_2$O source to the atmosphere. Our results suggest that ammonia-oxidizing archaea may be largely responsible for the oceanic N$_2$O source.

Tropospheric concentrations of nitrous oxide (N$_2$O) are currently 322 parts per billion and rising at a rate of ~0.25% per year

(1). Future projections for this radiatively active trace gas are uncertain, primarily because biological sources and sinks of N$_2$O are spatially and

temporally variable, and their mechanisms are not fully understood. Marine N$_2$O sources to the atmosphere are estimated to represent ~30% of total "natural" inputs, or ~4 Tg N$_2$O-N per year (2). Changes in the magnitudes of these sources depend on the mechanisms and controls of microbial N$_2$O production.

Marine N$_2$O production is thought to be carried out by ammonia-oxidizing bacteria (AOB)

[1]Department of Marine Chemistry and Geochemistry, Woods Hole Oceanographic Institution, Woods Hole, MA 02543, USA. [2]Joint Program in Chemical Oceanography, Massachusetts Institute of Technology–Woods Hole Oceanographic Institution, Woods Hole, MA 02543, USA.

*To whom correspondence should be addressed. E-mail: asantoro@umces.edu (A.E.S.); kcasciotti@stanford.edu (K.L.C.)
†Present address: Horn Point Laboratory, University of Maryland Center for Environmental Science, Cambridge, MD 21613, USA.
‡Present address: Department of Environmental Earth System Science, Stanford University, Stanford, CA 94305, USA.